ISSN 0020-4412, Instruments and Experimental Techniques, 2008, Vol. 51, No. 5, pp. 665–681. © Pleiades Publishing, Ltd., 2008.
Original Russian Text © A.D. Panov, V.I. Zatsepin, N.V. Sokolskaya, J.H. Adams, Jr., H.S. Ahn, G.L. Bashindzhagyan, J.W. Watts, J.P. Wefel, J. Wu, O. Ganel, T.G. Guzik, R.M. Gunashingha, J. Isbert, K.C. Kim, M. Christl, E.N. Kouznetsov, M.I. Panasyuk, E.S. Seo, J. Chang, W.K. H. Schmidt, A.R. Fazely, 2008, published in Pribory i Tekhnika Eksperimenta, 2008, No. 5, pp. 33–49.

NUCLEAR EXPERIMENTAL TECHNIQUE

Measuring the Deposited Energy by the Scintillation Calorimeter in the ATIC Experiment

A. D. Panov[a], V. I. Zatsepin[a], N. V. Sokolskaya[a], J. H. Adams, Jr.[b], H. S. Ahn[c], G. L. Bashindzhagyan[a], J. W. Watts[b], J. P. Wefel[d], J. Wu[c], O. Ganel[c], T. G. Guzik[d], R. M. Gunashingha[e], J. Isbert[d], K. C. Kim[c], M. Christl[c], E. N. Kouznetsov[a], M. I. Panasyuk[a], E. S. Seo[c], J. Chang[f,g], W. K. H. Schmidt[g], and A. R. Fazely[e]

[a] *Skobel'tsyn Institute of Nuclear Physics, Moscow State University, Moscow, 119992 Russia*
[b] *NASA Marshall Space Flight Center, Huntsville, AL 35812, USA*
[c] *University of Maryland, College Park, MD 20742, USA*
[d] *Louisiana State University, Baton Rouge, LA 70803, USA*
[e] *Southern University, Baton Rouge, LA 70813, USA*
[f] *Purple Mountain Observatory, Chinese Academy of Sciences, Nanjing, 210008 China*
[g] *Max-Planck Institute for Solar System Research, Katlenburg–Lindau, 37191 Germany*

Received December 27, 2007

Abstract—The purpose of the ATIC balloon experiment is to measure the energy spectra of primary cosmic rays with individual charge resolution from protons to iron over the energy range from ~50 GeV to 200 TeV. The particle energy is measured by a bismuth germanate (BGO) scintillation calorimeter. The procedure of calorimeter calibration is described, in particular, calibration of the temperature dependence of the calorimeter sensitivity using the data of in-flight measurements. A technique for determining the energy deposited in the calorimeter in view of the temperature dependence of its sensitivity is presented. The maximum systematic error in determining the deposited energy by the calorimeter is 10% or less, and the probable error is estimated at 6%.

PACS numbers: 95.85.Ry, 95.55.Vj

DOI: 10.1134/S0020441208050047

1. INTRODUCTION

The advanced thin ionization calorimeter (ATIC; see Fig. 1) consists of a silicon matrix composed of 4480 isolated silicon detectors with dimensions of 1.5×2.0 cm each and designed to determine the particle charge; a target composed of three 10-cm-thick graphite layers; three hodoscopes built up of 202 plastic scintillator bars 1 cm thick and 2 cm wide, which are arranged in six layers used to generate event triggers and as a supplementary detector of particle charges; and a fully active calorimeter composed of 320 bismuth germanate ($Bi_4Ge_3O_{12}$—BGO) crystals with dimensions of $25.0 \times 2.5 \times 2.5$ cm. The BGO crystals form eight layers with an area of 50×50 cm^2 each. Each crystal is viewed by an individual photomultiplier tube (PMT) of the Hamamatsu R5611 type. The depth of the calorimeter in a vertical plane is 18 cascade units; the thickness of the target together with the hodoscope scintillators is about three-quarters of the range of inelastic interaction for a proton. The ATIC spectrometer and the methods for calibrating it were described in detail in [1]; a method for determining the primary particle charge and the achieved resolution of the charge detector were presented in [2–4]. For the first time anywhere, a silicon detector matrix was used to measure the charge in high-energy cosmic rays [2]. Owing to the high segmentation of the charge detector, it provided a means for solving the reverse current (albedo) problem. The details of finding a solution to the albedo problem in the ATIC experiment, in particular, mathematical simulation of albedo particle production and passage and comparison of the theoretical results with the experiment, were presented in [5].

The ATIC had two successful stratosphere flights in Antarctica: one from December 28, 2000, to January 13, 2001 (the ATIC-1 test flight), and the other from December 29, 2002, to January 18, 2003 (the ATIC-2 science flight). The preliminary results from processing the ATIC-2 flight data were published in [6, 7]. The data concerning the ATIC-2 science flight will be discussed in what follows.[1]

In this paper, we provide a detailed description of a technique for measuring the energy deposited by cosmic particles in the BGO calorimeter of the ATIC spectrometer. In Section 2, we describe the procedure for calibrating the BGO calorimeter, which provides a

[1] While the paper was prepared for publication, the ATIC spectrometer had its third flight in Antarctica from December 26, 2007, to January 15, 2008. Processing of the flight data has just started.

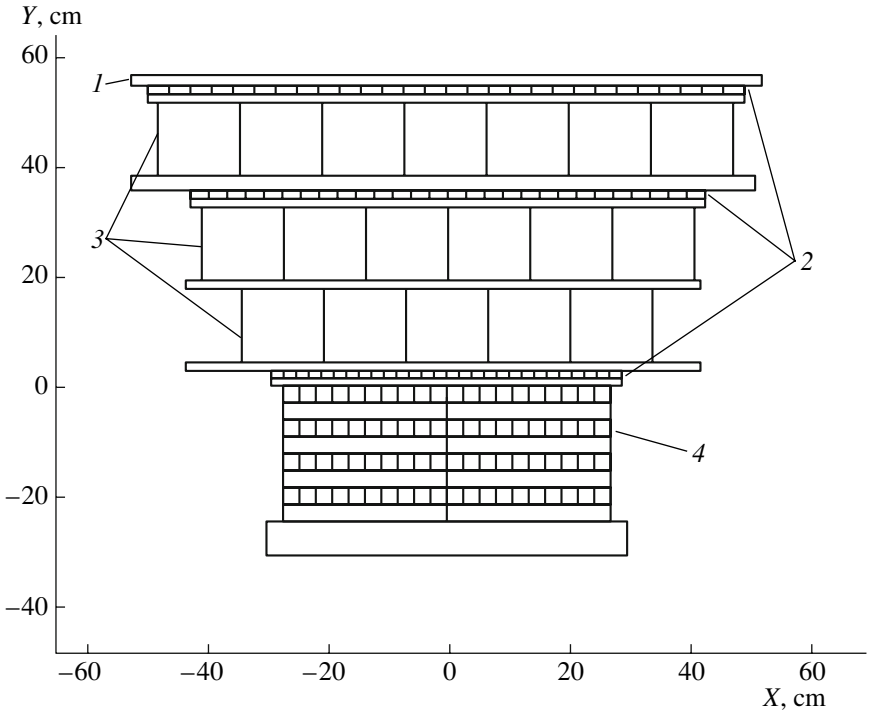

Fig. 1. Schematic diagram of the ATIC spectrometer (a side view): (*1*) silicon detector matrix, (*2*) scintillation hodoscopes, (*3*) graphite target, and (*4*) BGO calorimeter.

means for relating the data read out of the analog-to-digital converters (ADCs) to the energies deposited in the calorimeter crystals. Section 3 and its subsections are devoted both to determining the temperature dependence of the calorimeter sensitivity using different methods (and in different aspects) and to applying the appropriate temperature correction to the measured energies.

2. CALIBRATING THE BGO CALORIMETER

A system for detecting the energy deposited in the calorimeter must ensure measurements over a dynamic range of about 10^6 (from a few MeV to several TeV deposited in a single crystal). This is achieved by reading the PMT signal from three dynodes; as a result, three data readout channels with different sensitivities—channels R_0 (most sensitive), R_1 (medium), and R_2 (coarsest)—are created. The difference in the sensitivity of adjacent channels (R_0–R_1 or R_1–R_2) makes a value of a factor of 50, being dependent on the individual features of each PMT. For complete calibration of the calorimeter, we performed absolute calibration of channel R_0 for each crystal and, afterward, relative calibration of channel R_1 against channel R_0 and channel R_2 against channel R_1. Knowing the absolute calibration of R_0, one can also find the absolute calibration of channels R_1 and R_2. The procedures are described in detail in this section.

Absolute calibration of channel R_0 for each crystal was based on detection of atmospheric muons. In a preflight period, the instrument was in the on state over ~140 h (with a few breaks) and detected atmospheric muons from cosmic rays. The characteristic peak of ionization losses associated with the passage of muons was measured with a high statistical accuracy in the energy spectrum of each calorimeter crystal (Fig. 2). For each crystal, the position of the muon peak (the pulse height in terms of the ADC counts) was found by fitting the peak shape using the maximum likelihood method. The peak was fitted by the Gaussian function with the exponential background (all parameters of the Gaussian curve and all the background parameters—five parameters in total—were fitted) and by the function simulating the Landau distribution also with the exponential background. The major portion of the background fitted by the exponential is associated with the tail of the distribution function of the measuring channel pedestals and with the other causes (see below). Fitting by the exponential and the Landau function provides a difference in the peak position of ~5% of its height. An average of the values obtained using both these methods was selected to be the final value. As a result, the systematic error attributable to the method used to fit a peak in order to find its maximum does not exceed 2.5%. Apart from the experimental muon peak and the results of fitting, Fig. 2 also shows the measured pedestal of the electronic section, which has an individual value for each data acquisition chan-

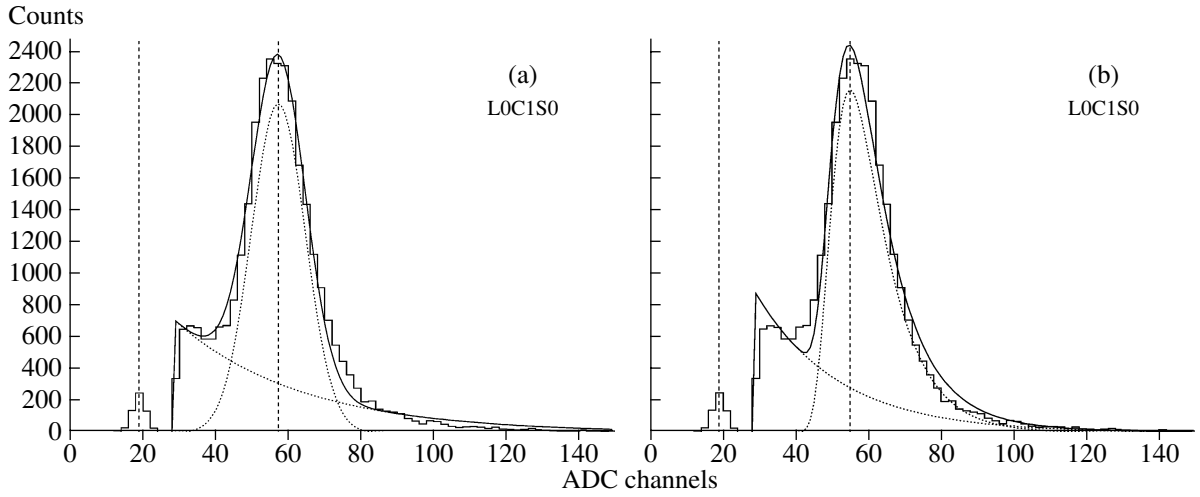

Fig. 2. Muon peak in one of the calorimeter crystals (layer 0, crystal no. 1, side 0). The measured peak is shown along with the fits (a) by the Gaussian function and (b) by the asymmetrical peak simulating the Landau distribution; in both cases, the peaks lie above the exponential background. The histogram shows the experimental data; the solid line, the results of fitting; the dashed-and-dotted line, the peak and the background determined separately; and the dashed line, the pedestal position of the electronic channel and the determined peak position. ADC denotes the analog-to-digital converter.

nel (a small peak on the left of the main muon peak) and is measured with a period of 1 h in special, artificially generated calibration events.

To refer the determined positions of the muon peak to a certain deposited energy (it is this operation that provides calibration of channel R_0 for each crystal, since it allows the energy per ADC count unit to be determined), a single-crystal peak of the energies deposited by atmospheric muons was simulated using the GEANT3 [8], GEANT4 [9, 10], and FLUKA [11, 12] codes. First, while solving a simple-geometry problem, we ascertained that the results of simulation using these three codes were almost identical: the GEANT4 and FLUKA codes provided exactly the same results, and the deposited energy calculated by means of the GEANT3 was 4% higher. Thereafter, using an accurate model of the ATIC spectrometer, the muon peak was simulated by the GEANT4 code in the actual geometry (a flat muon spectrum in the range from 500 MeV to 1 GeV, the angular distribution of muons described by function $\cos^2\Theta$, and simulation of the spectrometer's trigger for selected events). The model distribution of the energies deposited in a single crystal is shown in Fig. 3. In general, the distributions obtained for different crystals differ due to the specific features of their location in the entire configuration of the spectrometer; nevertheless, this difference is not so significant as to be taken into account when calculating the maxima of the distributions. The distribution averaged over all crystals is shown in Fig. 3.

The energy distribution has three main features. The first is the main peak attributable to the ionization losses of a muon incident on the upper face of the crystal and escaping from it through the lower face. The second feature is a flat plateau on the left of the main peak. This plateau is associated with muons that have only struck the crystal, penetrating into it through the upper face and escaping through the side surface. Events of this type also make their contributions to the background under the peak. The third feature is a narrow peak near zero of the deposited energy, which is mostly due to δ electrons produced by muons that have not passed through the crystal, traveling somewhere in the neighborhood of it. The position of the muon peak's main maximum is estimated at 23.2 MeV. It is this value that was used to calibrate individual crystals, since simulation conformed with a high accuracy to the experimental conditions under which the experimental single-crystal muon peaks had been recorded (Fig. 2).

The channel-to-channel calibration of pairs of channels R_0–R_1 and R_1–R_2 was based on flight data concerning records of primary cosmic ray events. In many cases, a single signal from a cosmic particle (the energy of which was deposited in a BGO crystal) is recorded at once in a pair of data acquisition channels—simultaneously in R_0–R_1 or R_1–R_2.

As a result, one can compare the gains in the relevant pairs of channels. Figure 4 demonstrates correlation between the pulse heights in pairs R_0– R_1 and R_1–R_2 for one of the BGO crystals. It is apparent that pairs of points fit the straight lines passing through the origin of coordinates, which allows one to easily determine the appropriate calibration coefficients by approximating the measured points by linear functions. Directly in Fig. 4, one can see that, as one passes from channel R_0 to R_1 and then from R_1 to R_2, the channel sensitivity decreases each time by a factor of 50. Of course, each BGO crystal has its own accurate values of the calibration coefficients.

Calibration using data from cosmic-ray events guarantees that it will be adequate to calculating the ener-

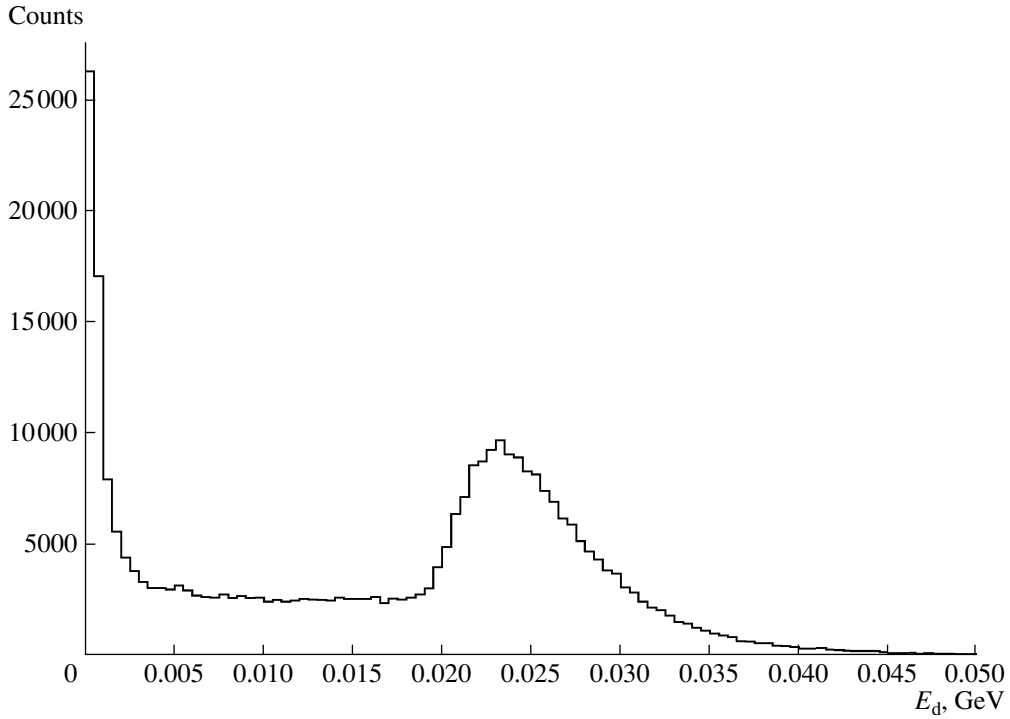

Fig. 3. Model single-crystal muon peak obtained using the GEANT4 code.

gies deposited in the calorimeter in similar scientific events. The ATIC spectrometer also permits the use of an alternative calibration technique, which consists in employing special calibration signals from the PMTs illuminated by light flashes from calibration LEDs. This technique also allows one to obtain signals that can be simultaneously detected in pairs of PMT channels. However, this technique is less reliable, since, in this case, the entire electronic system of the ATIC spectrometer may function in a different manner than when cosmic ray events are detected. In fact, two calibration techniques provide slightly different results. Nevertheless, LED-based calibration is also necessary; in our case, it is a kind of testing rather than calibration in a strict sense. It is used to check the spectrometer performance in a preflight period in order to make sure that all PMT channels are in operable condition. On the Earth, it is impossible without recourse to LEDs to obtain a signal that triggers a pair of channel at once. The signals produced by atmospheric muons passing through the spectrometer are too weak and induce a response only in channel R_0. For the signal to be recorded in a pair of channels simultaneously, it is necessary that these channels be triggered by a hard cosmic particle with a high deposited energy, which can occur only in the case of in-flight detection of primary cosmic particles.

3. TEMPERATURE CORRECTION OF THE BGO CALORIMETER SENSITIVITY

Each flight of the ATIC spectrometer was one full rotation around the South Pole approximately at the latitude of the south polar circle. Though the flights were performed during the polar day, the conditions of spectrometer illumination and heating were variable, since the angle of ascent of the Sun over the horizon varied according to the time of day and the albedo from the Earth's surface varied in the course of a flight. These facts, as well as the peculiarities of spectrometer performance, are responsible for the diurnal temperature variations and the long-term irregular changes in the temperature inside the spectrometer gondola (Fig. 5). The average flight temperature of the calorimeter was 18.46°C. Cosmic muons were detected over 20 h in the course of about four days prior to the ATIC-2 start, and these data were used thereafter to calibrate the sensitivity of the counting channel of the BGO calorimeter and the scintillation hodoscopes. The average calorimeter temperature during the calibration was 29.18°C. It is apparent that not only did the flight temperature vary within wide limits, but the calibration temperature also differed substantially from the average flight temperature. The quantum yield of BGO crystals is temperature-dependent, and the characteristics of the calorimeter's counting channel may also depend on temperature; therefore, for the signal amplitudes of the ADC in the calorimeter's counting channel to be correctly converted into the deposited energies, these data must be corrected for the current calorimeter temperature. The variations of the measured energy deposited in the calorimeter, caused by the temperature variations of the sensitivity, were within the limits of 20–30%. Taking into account that, in the first approximation, the differential spectrum of primary cosmic particles is repre-

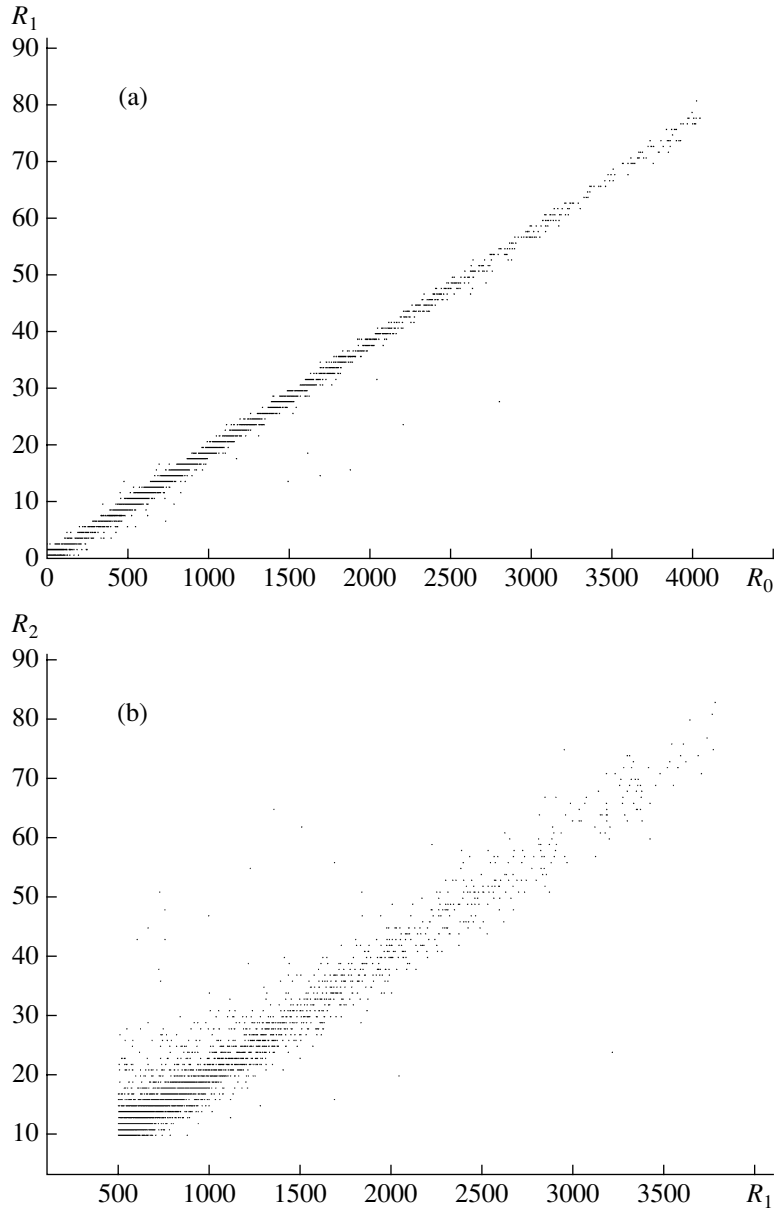

Fig. 4. For the interrange calibration: correlation between signals in pairs of channels (a) R_0–R_1 and (b) R_1–R_2.

sented by a power function with an exponent of about –2.75, one can easily see that a 30% error in determining the particle energy will lead to an increase by a factor of 1.6 in the error for the absolute particle flux intensity and, in addition, the spectral singularities (if they exist) will be offset from their characteristic positions. Results of measurements without a temperature correction turn out absolutely useless.

To obtain correct results, very careful temperature correction must be applied to the sensitivity of the calorimeter's counting channel, since the temperature effects are expected to be rather high. To do this, one must know the temperature dependence of the calorimeter sensitivity; moreover, the relevant coefficient should be determined from the flight or preflight data, since this would guarantee that the measured coefficient corresponds to the in-flight state of the spectrometer.

Since this problem had to be solved with a high degree of reliability, four different methods were used to find a solution to it. Agreement between results of different techniques can serve as evidence that these results are correct. Solving the problem in different ways was particularly important, because the temperature dependence of the calorimeter sensitivity appeared to be unexpectedly high. For this reason, the fact that the measured high value could not be attributed to

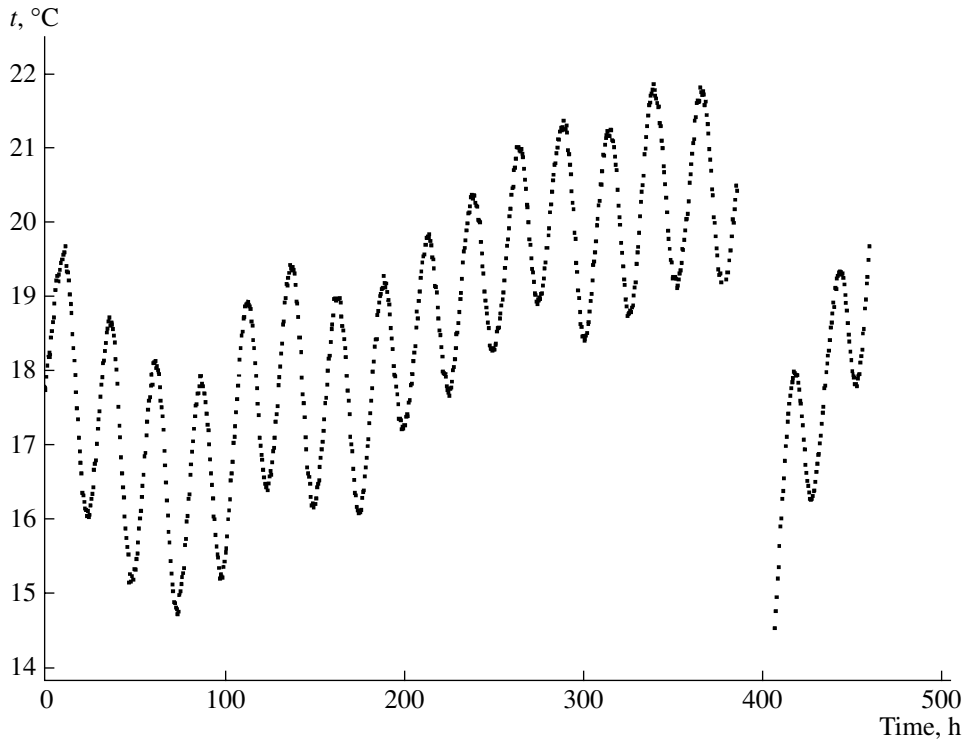

Fig. 5. Temperature of the BGO calorimeter (from now on, by the calorimeter temperature is meant the average of the readings of the ten sensors at the surface of the calorimeter) during the ATIC-2 spectrometer flight. Zero time corresponds to the instant when the spectrometer reached the rated altitude, the testing came to the end, and execution of the research program proper was started.

methodical effects had to be unambiguously determined.

There also exists a problem of thermal inertia of the calorimeter. The temperature sensors were fixed in place at several points at the surface of the BGO calorimeter, which was a parallelepiped with dimensions of $50 \times 50 \times 25$ cm. Since the temperature varied with a period of ~24 h in the course of a flight, questions arise as to what degree the temperature of the whole calorimetric section corresponds to the readings of the sensors and what the calibration error due to possible delay of the calorimeter temperature with respect to the sensor readings is. To answer these questions, one must measure the thermal relaxation time constant of the calorimeter (it is also desirable that this quantity be determined from the flight data) and estimate the possible methodological error due to the thermal inertia of the calorimeter. This is the second group of tasks that must be performed.

From now on, when the temperature sensitivity of the calorimeter is mentioned, we mean the coefficient describing the temperature dependence of the BGO calorimeter sensitivity. The next five subsections of Section 3 are devoted to four different methods for determining the temperature sensitivity of the calorimeter and the problems concerning its thermal inertia.

Finally, we note that the calorimeter temperature is measured by onboard temperature sensors, the accuracy of which is rather low (it is possible that the error is a few degrees). Nevertheless, this does not affect the accuracy of temperature correction applied to the deposited energy measured by the BGO calorimeter, since it is only important that this correction be self-consistent (i.e., the same thermometers must be used in measurements of the calorimeter temperature sensitivity and subsequent correction of the temperature errors).

3.1. Determining the Temperature Sensitivity of the Calorimeter from the Shift of the Muon Peaks in the Preflight Period

As noted above, the calorimeter was in the on state over ~140 h prior to the start; it detected secondary muons of cosmic rays in order to execute the calibration procedures and check the calorimeter performance. In this case, the temperature of the calorimeter was not constant (for random causes). The calorimeter temperatures measured over this period are presented in Fig. 6. The peak position in the distribution of the muon energies deposited in the BGO crystals has been related to the temperature. Four time intervals distinguished by either lowered or elevated temperature were considered (see Table 1 and Fig. 6).

The presence of a correlation between the temperature and the muon peak position is easily disclosed by eye. As an example, Fig. 7 demonstrates the shift of the

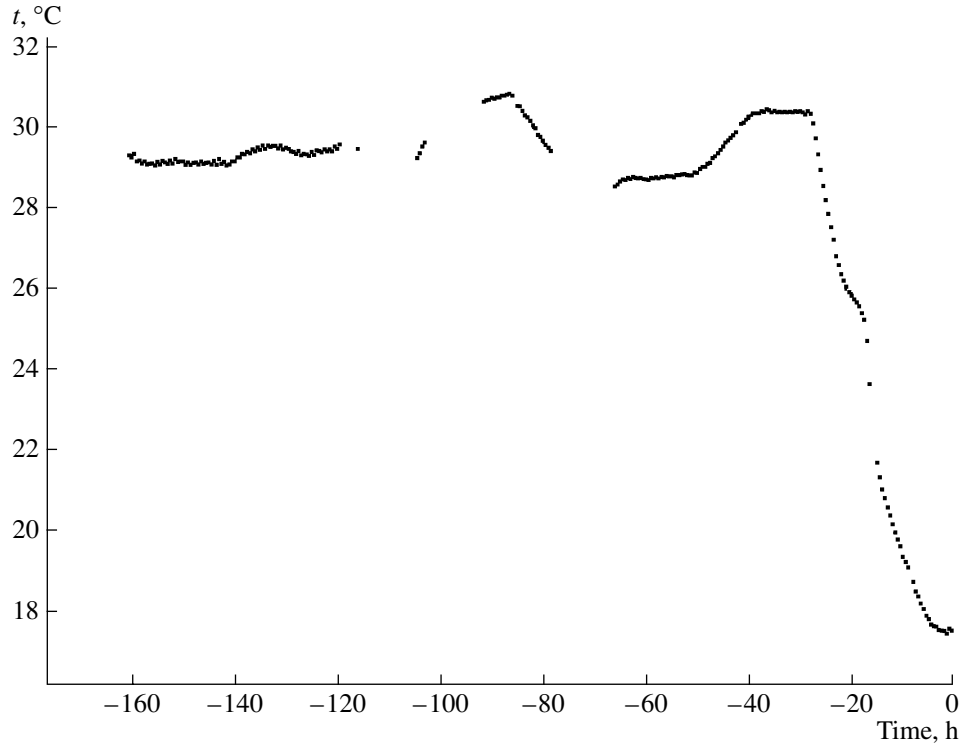

Fig. 6. Temperature of the BGO calorimeter before the flight and in the initial period of the flight. At the instant of time of about –30 h, the spectrometer was moved from the hangar out of doors; as a result, its temperature began declining. The instant of –20 h corresponded to the start; at the instant of –16 h, the rated flight altitude was attained.

muon peak after the temperature changes by 1.63°C, which takes place in going from time interval 3 to time interval 4 (see Table 1). It is apparent that the correlation has a negative character: an increase in the temperature is followed by a decrease in the calorimeter sensitivity.

To determine the temperature coefficient of the calorimeter sensitivity with a high degree of accuracy, the position of the muon peak was identified with zero of the derivative of the peak contour that was numerically determined using quadratic fit with a template, the width of which was approximately the full width at half-maximum of the peak. It should be noted that this method for finding the peak position can introduce a small (of about 2–4%) systematic error in determining the absolute position of the line. Nevertheless, this error is insignificant, since only relative shifts are important. (The temperature coefficient of the calorimeter sensitivity is expressed in terms of percent per degree Celsius.) This systematic error has no effect on the relative shifts, because the peaks being compared are identical in shape. The ascertained relationship between the temperature variations and the position of the muon peak is presented in Table 1, and the appropriate points are shown in Fig. 8. Processing of the points plotted in Fig. 8 provides the following value of the temperature sensitivity coefficient:

$$K_1 = -(2.63 \pm 0.38)\%/°\text{C}. \quad (1)$$

3.2. Determining the Temperature Sensitivity from the Difference in Position of the Preflight Muon Peak and the Flight Proton Peak for Events without Nuclear Interaction

Various trigger conditions were used to record events as the research program was executed. Apart from the other parameters, triggers differed in threshold of the energy deposited in the BGO calorimeter layers. The energy conditions selected for the main part of the research program were such that events were rejected in which a primary cosmic proton passed through the calorimeter without nuclear interaction and the total deposited energy constituted only the ionization loss of the proton. However, within a short time after the design flight altitude was attained, a trigger allowing

Table 1. Time intervals in the preflight period, the corresponding changes in the temperature, and the shifts of the muon peaks (for determining the temperature sensitivity coefficient of the calorimeter)

Interval no.	Interval, h	Δt, °C	ΔE, %
1	(–160, –140)	0.0 ± 0.20	0.0 ± 0.54
2	(–93, –83)	1.67 ± 0.23	–4.15 ± 0.62
3	(–62, –52)	–0.25 ± 0.17	0.45 ± 0.48
4	(–40, –30)	1.38 ± 0.19	–4.27 ± 0.53

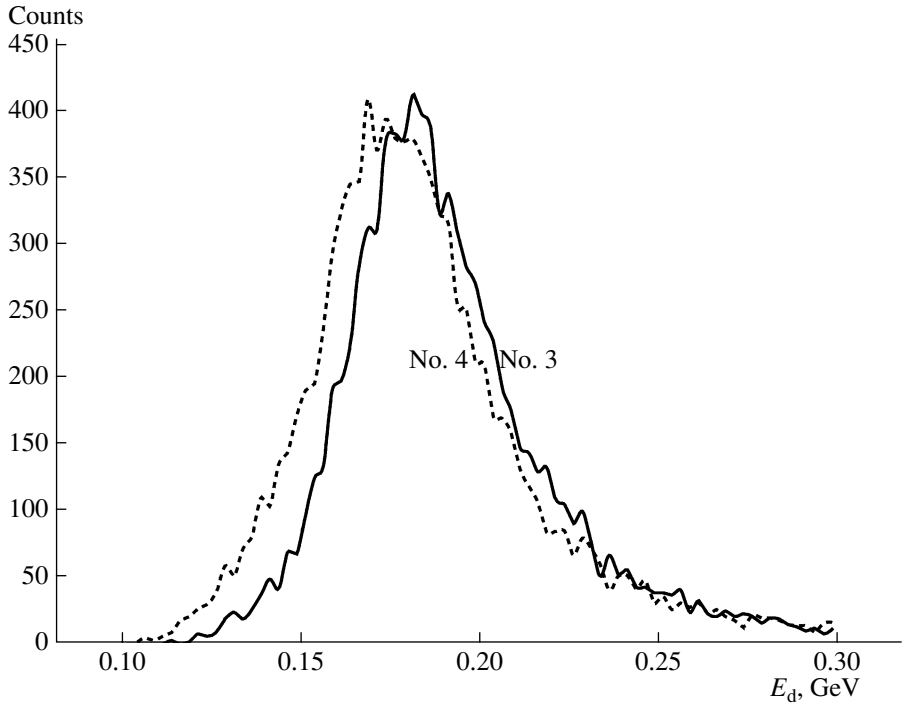

Fig. 7. Shift of the muon peak of the BGO calorimeter observed as the temperature changed from interval 3 to interval 4 (see Table 1).

the registration of any event without the energy threshold in the calorimeter was turned on for ~1 h (in the period from –13 h to –12 h) in order to adjust the system. Among events recorded in this period, one can easily recognize events in which a proton passed through the entire calorimeter without nuclear interaction; these events form a distinct peak in energy spectrum measured by the calorimeter. Such events are similar (but incompletely identical) to events from secondary cosmic muons detected on the Earth during preflight calibration. The peaks of secondary muons and primary noninteracting cosmic protons detected by the calorimeter are shown in Fig. 9. One can see a significant relative shift of the peaks, which can be attributed to the difference in the calorimeter temperature. Knowing the positions of the peaks and the respective temperature values, one can easily determine the temperature sensitivity coefficient of the calorimeter. Since the difference in position of the peaks is rather large, the coefficient should be determined according to the symmetrized formula

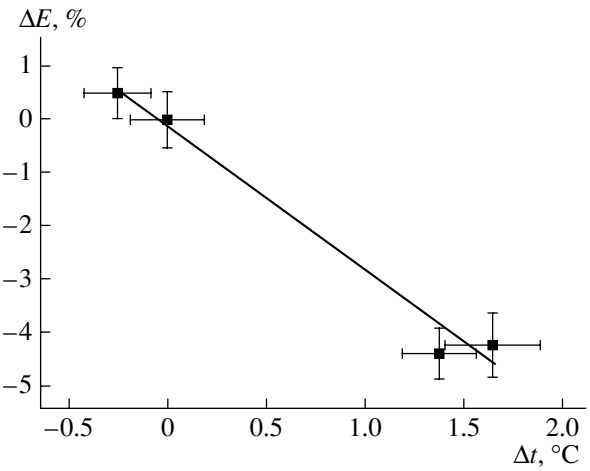

Fig. 8. Dependence of the muon peak position on the temperature variations (see Table 1). The shift of the peaks is presented in terms of percent of the peak position corresponding to time interval 1; the temperature shifts are also reckoned from the temperature corresponding to interval 1.

$$K = \frac{E_{post} - E_{pre}}{(E_{post} + E_{pre})/2} \frac{1}{T_{post} - T_{pre}}, \quad (2)$$

where E_{post} and E_{pre} are the post- and pretakeoff positions of the peaks (of the proton and muon peaks, respectively); T_{post} and T_{pre} are the respective temperatures. Substituting the measured values $E_{post} = 0.231 \pm 0.004$ GeV, $E_{pre} = 0.177$ GeV, $T_{post} = 20.29$°C, and $T_{pre} = 30.39$°C (for all values, except for the first one, the statistical errors are negligibly small) in Eq. (2), we obtain

$$K_2 = -(2.62 \pm 0.17)\%/°C. \quad (3)$$

This result virtually coincides with the value of K_1 in Eq. (1), which was to be expected; however, the physical ideas that form the basis for determining coefficients K_1 and K_2 differ only slightly, since K_1 was determined by comparing peaks of the same nature (muons

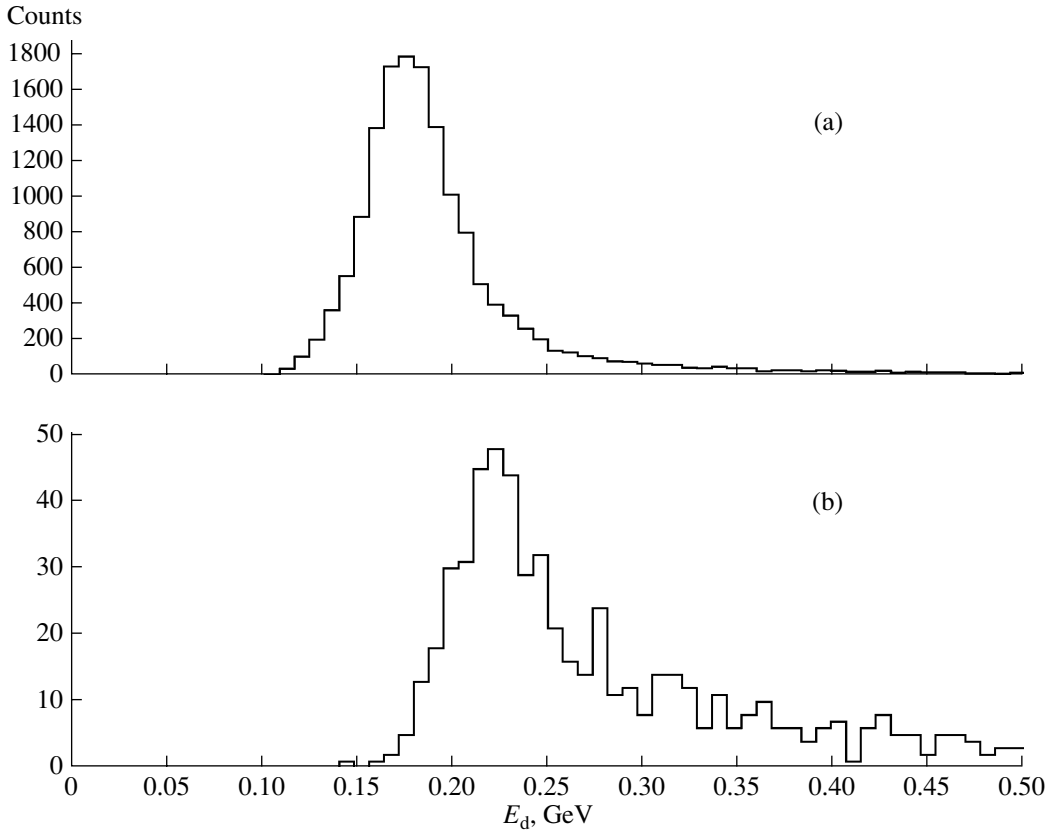

Fig. 9. (a) Muon peak of the energy deposited in the calorimeter, which was measured on the Earth in the interval of time from –40 to – 30 h, and (b) peak of noninteracting protons from primary cosmic rays.

with muons), while the peaks used to find K_2 had different nature (muons with protons).

3.3. Determining the Temperature Sensitivity of the Calorimeter from Diurnal Variations in the Positions of Proton and Helium Peaks for Events without Nuclear Interaction

The best option would be to use the temperature sensitivity coefficient of the calorimeter, measured directly during the flight in the course of research program execution. Such a coefficient is related to performed measurements by a direct dependence. For this purpose, one can try to monitor the variations in the sensitivity of the calorimeter caused by the diurnal and trend variations in its temperature during the flight (Fig. 5). However, there are some difficulties that make it impossible to directly realize the technique employed in the two previous subsections. The main problem consists in the fact that the energy thresholds used in the flight do not permit the detection of cosmic protons or helium nuclei passing through the entire calorimeter without nuclear interaction.

Nevertheless, a trigger denoted as LET30h was used in part of the flight time. This trigger provided a means for observing events with protons and helium nuclei suffering nuclear interactions below the uppermost calorimeter layer, but allowed a purely ionization signal (without nuclear interaction) from protons and helium to occur in this layer. Based on the temperature shifts of the appropriate peaks, one can determine the temperature sensitivity of the calorimeter, which will, however, characterize the upper layer of the calorimeter rather than the calorimeter as a unit. Nevertheless, even these data are useful for monitoring.

To extract proton and helium events, we used only those events in which the primary particle trajectories were reconstructed with a high degree of reliability and the charge was determined from the matrix of silicon detectors corresponding to a proton (when a proton peak was constructed) or a helium nucleus (for a helium peak). The total operation time of the LET30h trigger was 59 h; clearly discernible proton and helium peaks were obtained both for the whole interval and for individual 3-h subintervals (see Fig. 10). This has allowed us to organize 19 3-h intervals, for each of which the temperature of the upper layer (measured by the temperature sensors attached to the surface of the calorimeter near its upper layer) averaged over each time interval and the positions of the proton and helium peaks were determined. The time dependences obtained thereby are presented in Fig. 11. The synchronous vari-

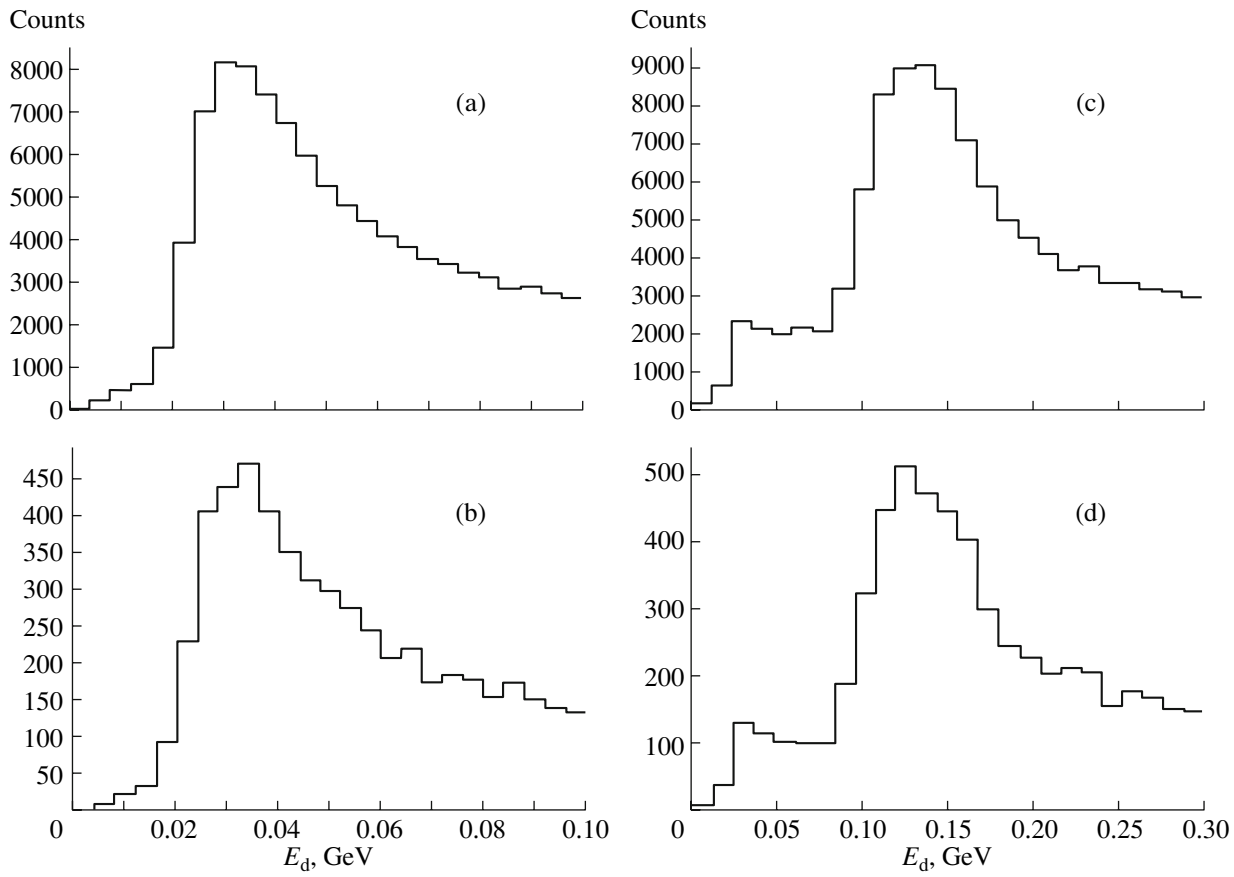

Fig. 10. (a) Gross proton peak acquired over 59 h in the upper calorimeter layer (layer no. 0); (b) proton peak acquired over 3 h (it corresponds to the first point in the plot in Fig. 11); (c) gross peak of helium nuclei, acquired over 59 h; and (d) helium peak acquired over 3 h.

ations of the peak positions and temperature are clearly discernible in the figure. Using these data, one can also plot the temperature dependence of the peak shift (Fig. 12) and, based on it, determine the respective temperature coefficients. Processing of the dependences in Fig. 12 using the least squares method provides

$$K_3^p = (2.62 \pm 0.41)\%/°\text{C}; \quad K_3^{\text{He}} = (1.94 \pm 0.20)\%/°\text{C}. \quad (4)$$

The statistical errors have not been calculated for each individual point on the plot; the final statistical errors in Eq. (4) were obtained a posteriori, from the scatter of plotted points. Coefficients K_3^p, and K_3^{He}, determined from the peaks of protons and helium nuclei, are in good agreement in view of the errors; therefore, it seems reasonable to use their weighed mean value:

$$K_3 = (2.07 \pm 0.18)\%/°\text{C}. \quad (5)$$

The coefficient obtained thereby is expected to be a little smaller than the true value, since the thermal inertia (the thermal relaxation time) of the calorimeter was ignored in calculation of it. The variations in the calorimeter sensitivity must lag behind the variations in the temperature measured by the sensors on the calorimeter surface, and the amplitude of variations in the calorimeter sensitivity will be slightly damped as compared to the case where the temperature variations are very slow. The effect of all these factors is expected to result in an underestimated value of the temperature sensitivity coefficient determined according to the procedure described in this subsection. In fact, coefficient K_3 in Eq. (5) appeared to be slightly smaller than K_1 in Eq. (1) and K_2 in Eq. (3). The corrections will be considered in Subsection 3.5.

3.4. Determining the Temperature Sensitivity of the Calorimeter by Correlation between the Counting Rate and the Pulse Height

A drawback of the technique described in Subsection 3.3 is the fact that result (5) corresponds only to the uppermost calorimeter layer. This drawback can be eliminated by monitoring the diurnal variations in the total counting rate of cosmic particles above a certain fixed threshold of energy deposited in the calorimeter.

The measured spectrum of energy deposited by particles passing through the aperture of the calorimeter is

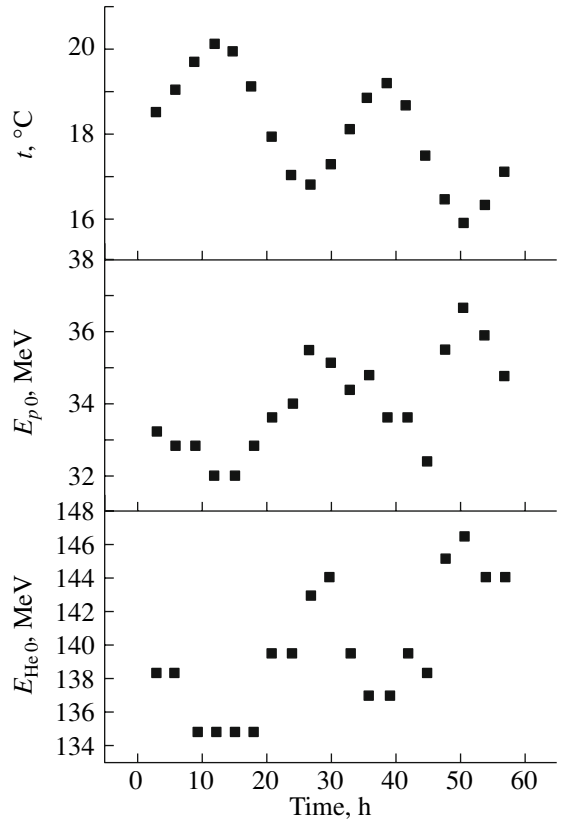

Fig. 11. Positions of the proton and helium nuclei peaks without nuclear interaction in the upper calorimeter layer and the diurnal temperature variations.

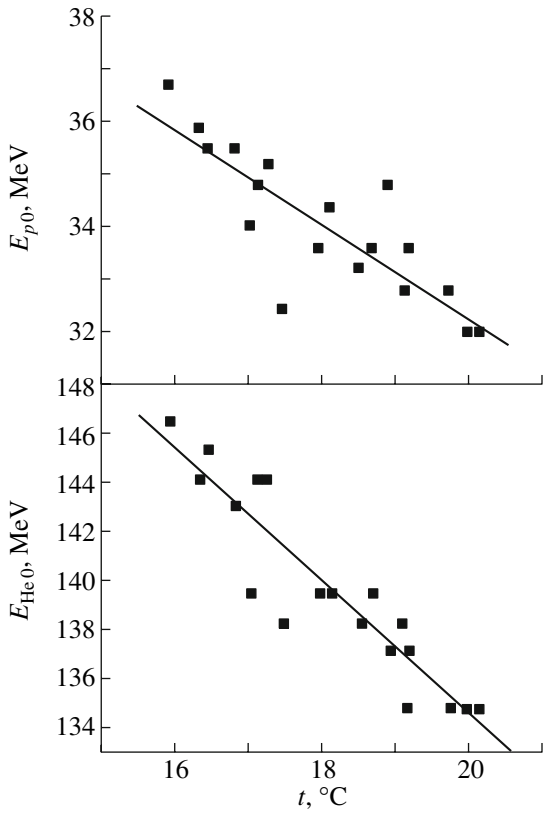

Fig. 12. Correlation of the proton and helium nuclei peaks without nuclear interaction in the upper calorimeter layer, with the diurnal temperature variations.

shown in Fig. 13. It is apparent that, above a 50-GeV threshold, the spectrum shape can be approximated by the power function:

$$D(E) = J_0 E^{-\gamma}, \tag{6}$$

where J_0 is the constant coefficient. The index of power obtained from analysis is $\gamma = 2.53$ (the statistical error is small). Assuming that the spectrum shape is exactly represented by the power function, one can easily determine the integral of the spectrum above certain threshold energy E_t:

$$S = \int_{E_t}^{\infty} J_0 E^{-\gamma} dE = J_0 \frac{E_t^{-(\gamma-1)}}{\gamma - 1}. \tag{7}$$

As the calorimeter sensitivity varies with temperature, all values of the measured energies change; therefore, the integral of the spectrum selected above threshold value E_t will also change. When calculating the integral according to Eq. (7), a small change in all the energies in the same proportion is equivalent to a change in the threshold that has the same value, but an opposite sign. If ΔT is the change in the temperature with respect to the a certain fixed reference temperature, it follows from the aforesaid that, in a linear approximation for the temperature dependence of integral S, we have

$$\begin{aligned} S(\Delta T) &= \frac{J_0 E_t^{-(\gamma-1)}}{\gamma - 1}(1 - K\Delta T)^{-(\gamma-1)} \\ &\approx \frac{J_0 E_t^{-(\gamma-1)}}{\gamma - 1}[1 + K(\gamma - 1)\Delta T], \end{aligned} \tag{8}$$

where K is the temperature sensitivity coefficient of the calorimeter in the sense in which it was used in Subsections 3.1–3.3. On the other hand, in the linear approximation, $S(\Delta T)$ has the form

$$S(\Delta T) = S_0(1 + K_S \Delta T), \tag{9}$$

where S_0 and K_S are constant coefficients. The value of K_S can be experimentally measured. Comparing Eqs. (8) and (9), we obtain

$$K = K_S/(\gamma - 1). \tag{10}$$

Figure 14 presents the time dependence of the integral counting above a 50-GeV threshold of deposited energies for cosmic particles passing through the calorimeter aperture. The integral counting was determined over successive 2-h intervals of data acquisition time. The acquisition time is the astronomical time minus the time spent by the spectrometer on engineering opera-

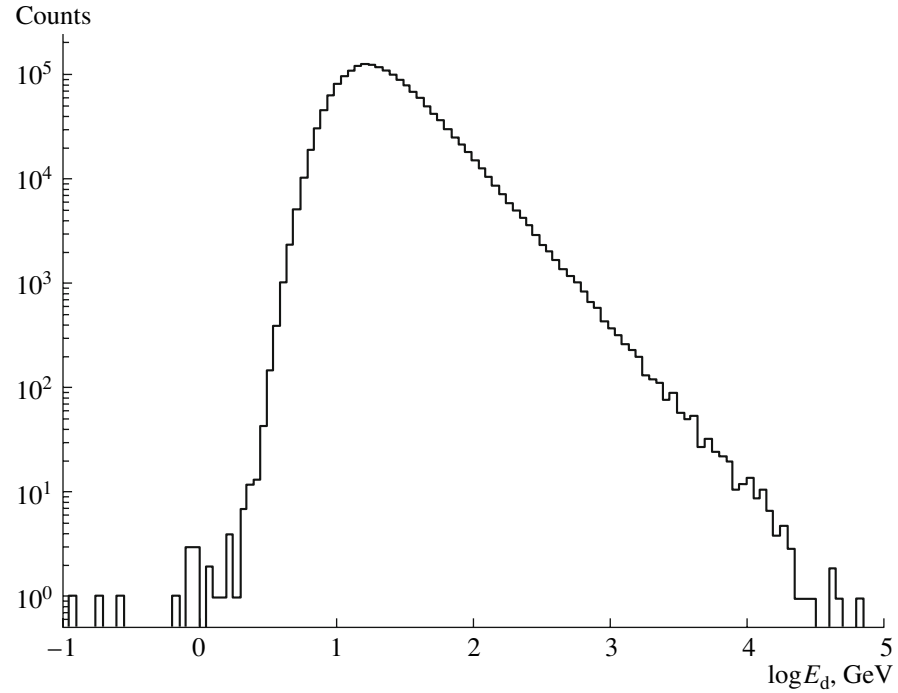

Fig. 13. Differential spectrum of the energies deposited in the calorimeter (in terms of counts per channel vs. the logarithm of the deposited energy). The complete statistics corresponding to one of the flight triggers was used. The spectrum precisely corresponds to the period of time used to determine the temperature sensitivity of the calorimeter from the variation in the counting rate (Subsection 3.4).

tions (testing, calibration, etc.), during which no scientific events were measured; the dead time of the calorimeter is not taken into account. In our case, taking into account the dead time is useless, since the counting rate varied only slightly; therefore, the variation of the contribution of the dead time to the acquisition time can be ignored. The anticorrelation between the temperature variations and the counting rate is easily distinguished in Fig. 14.

The temperature dependence of the total counting rate in the spectrum above a 50-GeV threshold is shown in Fig. 15. Clearly discernible cycles are seen in the figure. If Fig. 14 is carefully examined, one can see that the graphs of the temperature and the counting rate fail to vary precisely in antiphase and the variations in the counting rate lag behind the temperature variations. Therefore, the cycles in Fig. 15 are in the first approximation the result of superposition of two phase-shifted sinusoids and are nothing but Lissajous figures slightly smeared by a slow trend of the temperature. The lag is due to the finite thermal relaxation time of the calorimeter.

If all the points in Fig. 15 are approximated by a single straight line, coefficient K_S from Eq. (9) is $K_S = (3.79 \pm 0.40)\%/^\circ\mathrm{C}$; hence, using the index of power of the spectrum $\gamma = 2.53$ (see above) and Eq. (10), we find the temperature sensitivity coefficient of the calorimeter:

$$K_4 = (2.48 \pm 0.26)\%/^\circ\mathrm{C}. \qquad (11)$$

Arguments similar to those presented in this subsection suggest that the value of K_4 according to Eq. (11) is underestimated due to the neglect of the thermal inertia of the calorimeter. The corrections will be considered in the next subsection.

3.5. Thermal Relaxation Time and the Effective Temperature of the Calorimeter

Up to this point, when measuring the temperature sensitivity of the calorimeter, we used the temperature obtained by averaging the readings of several sensors located at the calorimeter surface. Let us assume that this temperature is the temperature of a thermostat with infinitely high heat capacity, which we call the *environment*. The temperature of the environment is denoted by X. The calorimeter is thought to have intrinsic effective temperature Y, which directly affects its sensitivity to deposited energy, averaged throughout the calorimeter volume. Let us consider that the environmental temperature is the prescribed function of time $X(t)$ and suppose that the calorimeter temperature is governed by heat transfer from the environment to the calorimeter. Under the assumption that the region under consideration is characterized by linear heat transfer, the rate of relaxation of the calorimeter temperature to the environmental temperature is expected to be proportional to the difference of the respective temperatures:

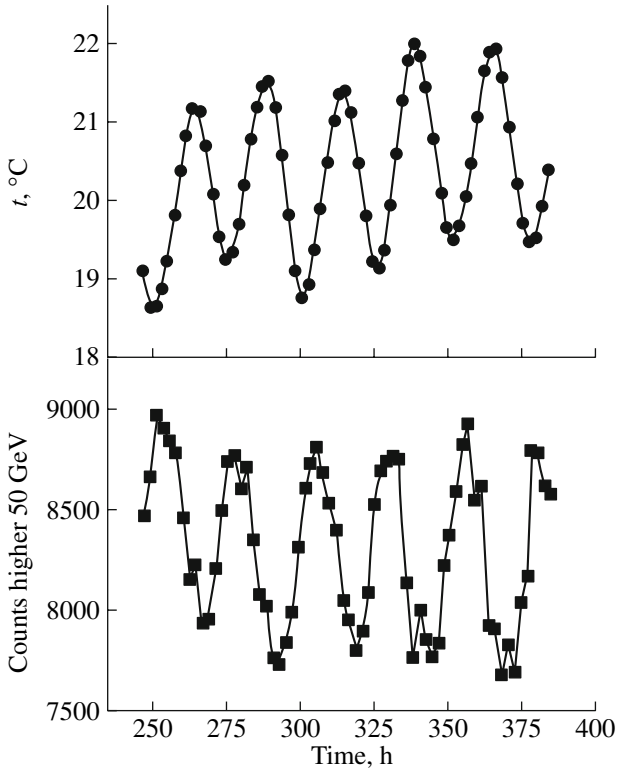

Fig. 14. Time dependences both of the counting rate of cosmic particles that passed through the spectrometer aperture and deposited energies of >50 GeV and the calorimeter temperature.

$$\frac{dY(t)}{dt} = \lambda[X(t) - Y(t)], \quad (12)$$

where λ is the thermal relaxation constant of the calorimeter. The corresponding relaxation time is $\tau = 1/\lambda$. At predetermined environmental temperature $X(t)$ and predetermined initial condition $Y(t_0)$, Eq. (12) completely defines the calorimeter temperature for $t > t_0$.

Our aim is to determine the relaxation time of the calorimeter from the flight data. This problem can be solved proceeding from the observed phase shift between the diurnal variations of the environmental temperature and the respective thermal response of the calorimeter. The simplest way is to use the data on the variations in the integral of the counting rate of cosmic particles (Subsection 3.4 and Fig. 15). The temperature of the environment is assumed to vary according to the harmonic law; therefore, Eq. (12) takes the form

$$\frac{dY(t)}{dt} = \lambda[(X_0 + A_x \sin\omega t) - Y(t)]. \quad (13)$$

Let us find a solution to Eq. (13), which describes the stationary oscillations of the calorimeter temperature. One can easily make sure that such a solution has the form

$$Y(t) = X_0 + A_Y \sin\omega(t - \delta t), \quad (14)$$

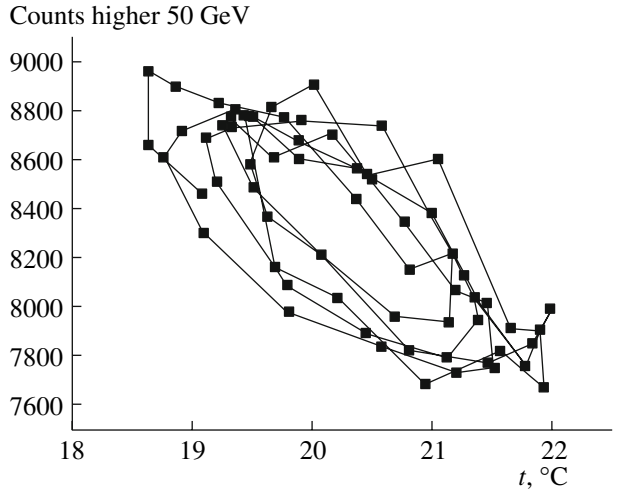

Fig. 15. Temperature dependence of the counting rate of cosmic particles that passed through the spectrometer aperture and deposited energies of >50 GeV.

where

$$\delta t = \frac{1}{\omega}\arctan\frac{\omega}{\lambda}, \quad (15)$$

$$A_Y = \frac{\lambda}{\omega\sin\omega\delta t + \lambda\cos\omega\delta t}A_X. \quad (16)$$

Equation (14) describes the sinusoid shifted in time by δt and with slightly suppressed amplitude A_Y. If the value of time shift δt in the pattern of stationary oscillations is known beforehand, Eq. (15) allows us to find relaxation constant λ and, therefore, relaxation time τ:

$$\tau = \frac{1}{\omega}\tan\omega\delta t. \quad (17)$$

Now, assuming that the temperature dependence in Fig. 15 is approximated by the sinusoid and measuring time shift δt between the temperature curve and the calorimeter response curve, we can easily find relaxation time τ from Eq. (17).

The curves presented in Fig. 15 were used to determine the experimental value of δt. The δt value maximizing the module of the correlation coefficient was sought for these curves:

$$|\mathrm{corr}[X(t), Y(t + \delta t)]| = \left|\frac{\langle[X(t) - \bar{X}][Y(t + \delta t) - \bar{Y}]\rangle}{\sqrt{\langle[X(t) - \bar{X}]^2\rangle}\sqrt{\langle[Y(t + \delta t) - \bar{Y}]^2\rangle}}\right| \longrightarrow \max. \quad (18)$$

As a matter of fact, experimental function $Y(t)$ is defined by separate points for fixed instants of time; therefore, a linear interpolation between the measured points was used to determine the values of $Y(t + \delta t)$ for arbitrary shifts δt.

The dependence of correlation coefficient (18) on shift δt, which corresponds to the curves in Fig. 15, is

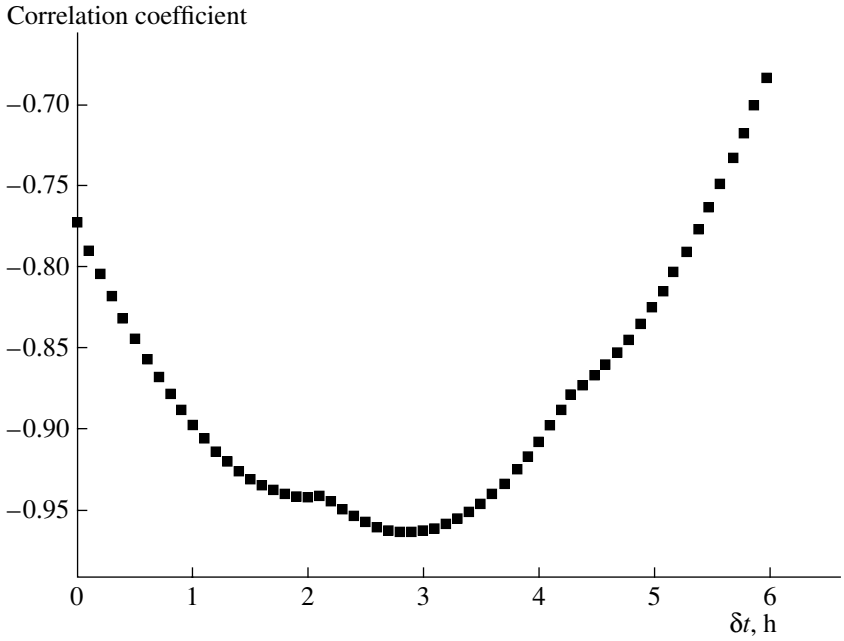

Fig. 16. Dependence of the correlation coefficient of the curves in Fig. 15 on time shift δt.

presented in Fig. 16. The maximum of the correlation coefficient module is attained for $\delta t = 2.88$ h. It is this value that acts as the experimental estimate for the shift of the temperature curve and the calorimeter response curve.

It is rather difficult to find the experimental error for this value, since this error is composed of a sophisticated combination of statistical fluctuations and methodical effects. However, there is no need for accurate estimation of the error, since the differences of the environmental temperature from the effective calorimeter temperature give rise only to minor changes in the temperature correction of the calorimeter sensitivity; therefore, the errors in determining δt give rise to corrections of the second order of infinitesimal. To coarsely estimate the scale of the error, an analysis similar to the analysis described above was performed for the other leg of the flight. (The event trigger with the other energy thresholds was used on this leg.) However, this leg was several times shorter than the time interval used for the basic estimate; therefore, the accuracy was consciously worse. For the new leg, we obtained $\delta t = 3.31$ h. The difference of ~0.4 h in the estimates can be considered as the upper estimate for the error of basic value $\delta t = 2.88$ h. This accuracy fully satisfies us.

The average duration of the day's period corresponding to Fig. 15 was 25.1 h. (It differs from 24 h, since the satellite moved around the pole in the direction opposite to the Earth's rotation.) Using this value, value $\delta t = 2.88 \pm 0.4$ h, and Eq. (17), one can easily obtain the calorimeter relaxation time

$$\tau = 3.5 \pm 0.5 \text{ h}. \quad (19)$$

In Eq. (19), the error value should be considered as the upper estimate of the error.

Estimate of the relaxation time (19) allows us, based on the in-flight temperature measurements, to reconstruct the effective calorimeter temperature for each instant of time and use it thereafter in temperature correction of the calorimeter sensitivity. This can be done if we solve Eq. (12) with function $X(t)$—the environmental temperature determined by the actual in-flight readings of the temperature sensors. The simplest way to solve this equation is to present function $X(t)$ by a piecewise-linear spline. Equation (12) with linear function $X(t)$ admits of an exact solution. Assuming that the initial conditions at instant of time t_0 are $Y(t_0) = Y_0$ and function $X(t)$ on segment $[t_0, t_1]$ is defined by equation $X(t) = a + bt$, we can find for instant of time t_1

$$\begin{aligned} Y(t) &= a + b(t_1 - \tau) \\ &+ \{Y_0 - [a + b(t_0 - \tau)]\} e^{-\lambda(t_1 - t_0)}. \end{aligned} \quad (20)$$

Therefore, Eq. (12) with function $X(t)$ in the form of a linear spline can be exactly solved segment by segment, actually without recourse to numerical methods. In Fig. 17, the environmental temperature measured by the sensors at the surface of the calorimeter is compared to the effective calorimeter temperature determined by solving Eq. (12).

Now, we can return to correction of the temperature sensitivity coefficients of the calorimeter that were obtained in Subsections 3.3 and 3.4. Correction implies that exactly the same analysis that was performed in these subsections should be repeated, but the environmental temperature directly measured by the tempera-

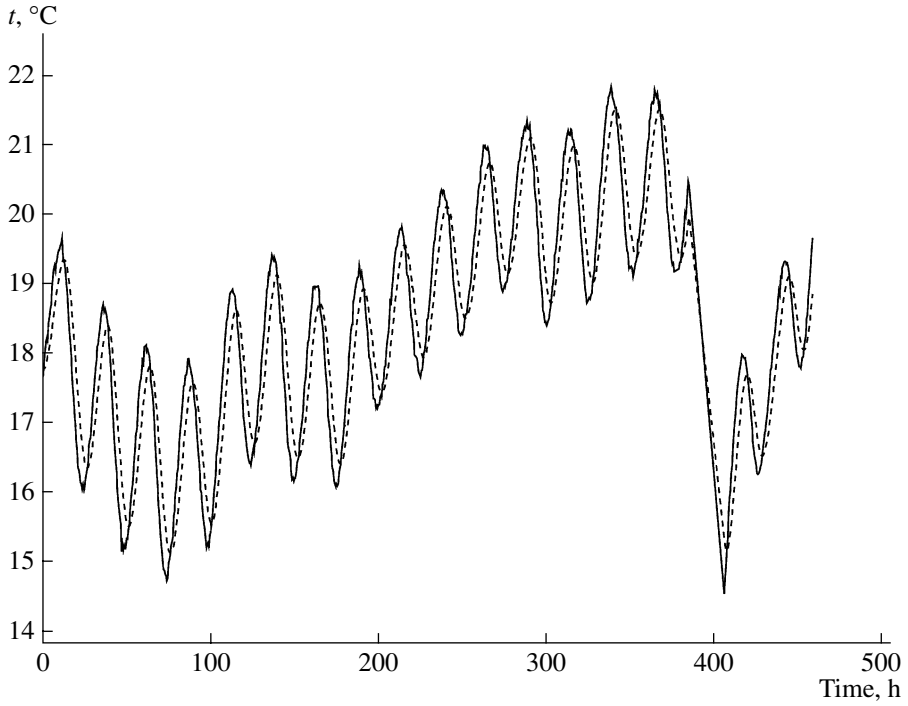

Fig. 17. Temperature measured by the sensors (a solid line) and the effective calorimeter temperature (a dashed line), obtained by solving Eq. (12).

ture sensors must be replaced by the reconstructed effective temperature of the calorimeter. This analysis provides the following corrected values of the temperature sensitivity coefficients:

$$K_3^{\text{corret}} = (-2.33 \pm 0.17)\%/°\text{C}, \quad (21)$$

$$K_4^{\text{corret}} = (-2.66 \pm 0.26)\%/°\text{C}. \quad (22)$$

4. DISCUSSION OF THE RESULTS

The final results from measuring the temperature sensitivity coefficient of the calorimeter using different methods are presented in Table 2. It is apparent that all the values are in good agreement with each other. Note that the results obtained with methods 1, 2, and 4 coincide with a much higher accuracy than can be attributed to measurement error. Since the methods for calculating the errors are thought to be fully adequate, this may be caused by a rare statistical fluctuation.

The first method (see Subsection 3.1), which is based on the muon peak shift measured in the preflight period, is the most direct and reliable. The temperature varied very slowly in these measurements; therefore, the calorimeter was virtually in thermal equilibrium with the environment; hence, the directly measured temperature of the environment also corresponded to the effective temperature of the calorimeter itself. In this case, the nature of the measured value remained unchanged, by contrast to the second method (Subsection 3.2), in which the position of the muon peak compared to that of the proton peak. In the latter case, the measurements were taken under quite dissimilar conditions—in a hangar and in flight at different pressures inside the gondola. Taking this fact into account, value $K_1 = -(2.63 \pm 0.38)\%/°\text{C}$ obtained from the muon peak positions was selected for applying temperature correction as the basic value of the temperature sensitivity coefficient; all the others (Table 2) were considered to corroborate the correctness of this value. The agreement between all values indicates that there were no significant extraneous factors that could give rise to errors in a temperature correction in the flight. Note that the coefficient determined from the diurnal variation in the proton and helium peaks (Subsection 3.3) differs slightly in its nature from the other measurements, since it characterizes only the upper layer of the calorimeter rather than the entire calorimeter. As a matter of fact, as is seen from Table 2, its value differs only slightly from the other values. (However, this difference virtually lies within the limits of experimental errors.)

All the techniques described, from the calorimeter calibration to the techniques concerned with the temperature correction and thermal inertia of the calorimeter, permit spectrum measurements of energies deposited by different sorts of cosmic particles. Figure 18 presents the spectrum of energies deposited by cosmic protons in the calorimeter, which was obtained without a correction for the temperature sensitivity of the calorimeter and with the corrections based on the environmental temperature and the effective calorimeter tem-

Table 2. Temperature sensitivity coefficients of the calorimeter, determined using different methods

Subsection	Method	Coefficient, %/°C
3.1	Slow variation of the muon peak position in the preflight period	–2.63 ± 0.38
3.2	Comparison of the preflight muon peak with the flight proton pea	–2.62 ± 0.17
3.3, 3.5	Diurnal variations in the positions of the proton and helium peaks (only for the upper calorimeter layer)	–2.33 ± 0.17
3.4, 3.5	Diurnal variations in the counting rate of cosmic particles above the 50-GeV threshold of deposited energy	–2.66 ± 0.26

perature being applied. It is apparent that the absence of the temperature correction leads to very crude errors in the spectrum (more than 50% in the majority of spectrum points), which, as was expected (see Introduction), makes the uncorrected experimental results useless. At the same time, corrections based on the use of the environmental temperature and the effective calorimeter temperature lead to almost identical results. This is caused by the fact that the difference of the effective temperature from the environmental temperature has a character of oscillations around zero (with a period of ~25 h) with a small amplitude (slightly greater than 1°C), and the effect of these oscillations is averaged over a long flight time (several hundreds of hours). Since the energy resolution of the calorimeter (25–30%) is not very high, these oscillations have almost no effect on the results. Note that the spectrum in Fig. 18 fails to be a spectrum of primary energies of cosmic protons. The ATIC calorimeter is thin; i.e., it measures only a portion of the primary particle energy. To obtain the original energy spectrum of particles, one must solve the inverse problem known as deconvolution. A description of the relevant technique in the ATIC experiment was presented in [13].

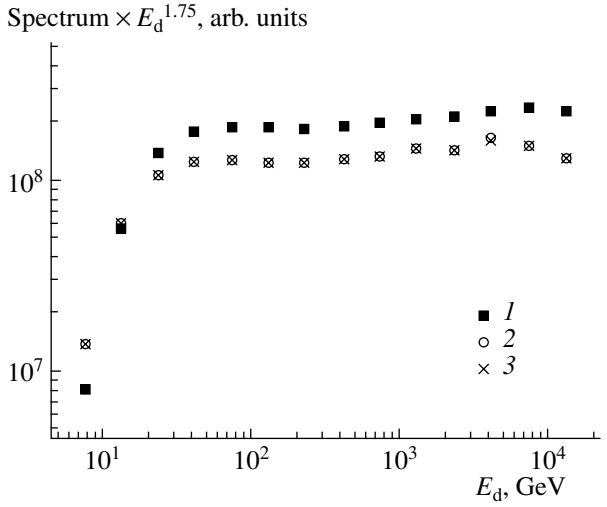

Fig. 18. Spectrum of the energy deposited by cosmic protons in the calorimeter (*1*) without a correction for the temperature sensitivity of the calorimeter being applied and with the corrections based (*2*) on the temperature of the environment and (*3*) on the effective calorimeter temperature.

Let us estimate the possible methodical error in measuring the energy deposited by cosmic particles in the BGO calorimeter of the ATIC spectrometer. As noted in Section 2, there is an uncertainty in referencing the position of the muon peak to a fixed ADC channel. This uncertainty, caused by the ambiguity in selection of the function for fitting the shape of the single-crystal muon peak, may be as great as 2.5%. The difference between the mean flight temperature and the calibration temperature being ~10°C, a 0.38% error of the temperature sensitivity coefficient of the calorimeter may cause a 3.8% error in determining the deposited energy. The uncertainty attributable to simulation of the muon's deposited energy, estimated by the difference in results obtained using the GEANT3, GEANT4, and FLUKA codes (see Section 2) is 4% or under. Therefore, the maximum possible methodical error does not exceed 10%, while the probable error is 6%.

Measurements of the temperature sensitivity were also performed under laboratory conditions [14] after the ATIC-2 flight. The technique used in the laboratory prohibits direct comparison of the laboratory data to the results of in-flight measurements presented in this paper. This is caused by the fact that the individual temperature sensitivity of each crystal (together with its electronics) was determined during the laboratory measurements and the external thermometer of the laboratory thermostat was used to measure the temperature instead of the flight temperature sensors. To perform comprehensive comparison with the data presented in this paper, it is necessary that the relationship between the thermometer of the laboratory thermostat and the readings of the flight sensors be ascertained and a nontrivial conversion of the results obtained for each individual crystal to the integral value characterizing the entire calorimeter be effected. This has not yet been done; however, we can assert with a high degree of reliability that the scales of the values measured in the laboratory fully agree with the data obtained during the flight.

ACKNOWLEDGMENTS

This work was supported by the Russian Foundation for Basic Research (grant no. 05.02.16222) and the National Aeronautics and Space Administration of the United States (grants nos. NNG04WC12G, NNG04WC10G, and NNG04WC06G).

REFERENCES

1. Guzik, T.G., Adams, J.H., Ahn, H.S., et al. (ATIC Collab.), *Adv. Space Res.*, 2004, vol. 33, p. 1763.
2. Adams, Jr., J.H., Bashindzhagyan, G.L., Zatsepin, V.I., et al., *Prib. Tekh. Eksp.*, 2001, no. 4, p. 38 [*Instrum. Exp. Tech.* (Engl. Transl.), no. 4, p. 455].
3. Zatsepin, V.I., Adams, Jr., J.H., Ahn, H.S., et al. (ATIC Collab.), *Izv. Ross. Akad. Nauk, Ser. Fiz.*, 2003, vol. 66, p. 1631.
4. Zatsepin, V.I., Adams, Jr., J.H., Ahn, H.S., et al. (ATIC Collab.), *Nucl. Instrum. Methods Phys. Res. A*, 2004, vol. 524, p. 195.
5. Sokol'skaya, N.V., Adams, Jr., J.H., Ahn, H.S., et al. (ATIC Collab.), *Yad. Fiz.*, 2005, vol. 68, p. 1225 [*Phys. At. Nucl.* (Engl. Transl.), vol. 68, p. 1176].
6. Zatsepin, V.I., Adams, Jr., J.H., Ahn, H.S., et al. (ATIC Collab.), *Izv. Ross. Akad. Nauk, Ser. Fiz.*, 2004, vol. 68, p. 1593.
7. Panov, A.D., Adams, Jr., J.H., Ahn, H.S., et al. (ATIC Collab.), *Advances in Space Research*, 2006, vol. 37, p. 1944.
8. Brun, R., Brayant, F., and Maire, M., *GEANT User Manual*, Geneva: CERN, 1984.
9. Agostinelliae, S., Allison, J., Amako K., et al, *Nucl. Instrum. Methods Phys. Res. A*, 2003, vol. 506, p. 250.
10. Allison, J., Amako, K., Apostolakis, J., et al., *IEEE Trans. Nucl. Sci.*, 2006, vol. 53, p. 270.
11. Fassŏ, A., Ferrari, A., Roesler, S., et al., Abstracts of Papers, *Computing in High Energy and Nuclear Physics 2003 Conference (CHEP2003)*, La Jolla, California, USA: eCONF, 2003, vol. C0303241; hep-ph/0306267.
12. Fassŏ, A., Ferrari, A., Ranft, J., and Sala, P.R., *Nos. CERN-2005-10, INFN/TC_05/11, SLAC-R-773*, Geneva, 2005.
13. Batkov, K.E., Panov, A.D., Adams, Jr., J.H., et al. (ATIC Collab.), Abstracts of Papers, *Proc. 29th Int. Cosmic Ray Conf*, Pune, 2005, vol. 3, p. 353.
14. Isbert, J., Adams, Jr., J.H., Ann, H.S., et al. (ATIC Collab.), Abstracts of Papers, *Proc. 29th Int. Cosmic Ray Conf*, Pune, 2005, vol. 3, p. 397.